ACS OMEGA

http://pubs.acs.org/journal/acsodf

Article

Optical Properties of a $CsMnBr_3$ Single Crystal

Yingzhuang Xu, Junzi Li, Fuli Zhao, Yang Gao,* Rui Chen, and Tingchao He

Cite This: *ACS Omega* 2022, 7, 29415−29419

Read Online

ACCESS | Metrics & More | Article Recommendations | Supporting Information

ABSTRACT: Lead-free perovskite materials with good stability are promising for various applications. In order to explore their application in optoelectronic devices, it is essential to investigate their fundamental optical properties. In this work, we have synthesized a $CsMnBr_3$ single crystal (SC) with red emission at ∼621 nm and studied their optical properties. Through the measurement of temperature-dependent photoluminescence (PL) spectra, it is found that a phase transition occurs at approximately 100 K in the SC, which is absent in the $CsMnBr_3$ nanocrystals (NCs). Furthermore, the SC exhibits stronger electron and longitudinal optical phonon coupling strength than that of the NCs at low temperatures. In addition, under the resonant excitation at 600 nm, the SC possesses strong saturable absorption property, with a modulation depth of ∼27%. Interestingly, the SC also exhibits a large two-photon absorption coefficient of ∼0.035 cm GW^{-1} at 800 nm and an excellent optical limiting behavior. The experimental results indicate that the $CsMnBr_3$ SC is a class of excellent environmentally friendly optoelectronic materials.

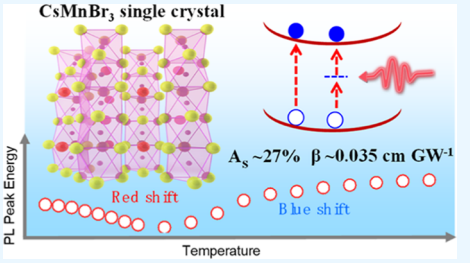

INTRODUCTION

All inorganic perovskite materials ($CsPbX_3$, X = Cl, Br, and I) have been widely used in various applications, such as light detection, photovoltaic cell, and laser, because of their excellent optoelectronic properties, including high photoluminescence quantum yield (PLQY), widely tunable PL emission, and large absorption cross section.[1] However, the intrinsic toxicity of these materials greatly hinders their practical applications. Therefore, to reduce the toxicity of the materials, researchers have synthesized various lead-free perovskite materials, with Cu^{2+}, Sn^{2+}, and Bi^{3+} as substitutes for Pb^{2+},[2−4] and developed their application in various optoelectronic devices.

In recent years, Mn^{2+} has been continuously studied as a dopant and an alternative element for Pb^{2+} due to its unique luminescence,[5,6] which has green emission in the form of tetrahedral coordination and red emission in the form of octahedral coordination. As a newly emerging lead-free perovskite material, $CsMnBr_3$ has attracted intensive research interest.[7,8] However, although the research on $CsMnBr_3$ nanocrystals (NCs) is relatively adequate, $CsMnBr_3$ single crystals (SCs) have not been extensively studied. Compared with the NC counterparts, SCs are more suitable for preparing large-area optoelectronic devices.[9] The study on the optical properties of $CsMnBr_3$ SCs is a prerequisite for realizing their relevant application. For example, the electron−phonon coupling effect in $CsMnBr_3$ SCs can be investigated through the measurement of the temperature-dependent PL spectrum, which is crucial for developing high-efficiency photovoltaic and laser devices.[10,11] Investigating the nonlinear optical (NLO) behavior of $CsMnBr_3$ SCs is important to develop their applications in Q-switching and mode-locking techniques[12,13] and frequency upconversion laser.[14,15] Nevertheless, there is still a lack of in-depth investigation on these fundamental optical properties of $CsMnBr_3$ SCs, which is unfavorable to expand their various applications.

In this work, we synthesized a $CsMnBr_3$ SC and studied its optical properties. Phase transition was observed at a temperature of approximately 100 K. In addition, it was found that the $CsMnBr_3$ SC exhibited strong saturable absorption and two-photon absorption (TPA).

METHODS

Sample Preparation. The $CsMnBr_3$ SC was obtained through a slow evaporation method described in the previous literature.[7] Briefly, 0.55 mmol CsBr and 1 mmol $MnBr_2$ were added to the mixed solution of water and hydrobromic acid (19:1 in weight) and then heated to 40 °C in ambient conditions. As a result, the $CsMnBr_3$ SC with a size in millimeter level was formed after storage for 5 days. $CsMnBr_3$ NCs were prepared through a hot-injection method according to a previous procedure with a slight modification.[8] During the synthesis process, 1-octadecene was used as a solvent, while oleic acid and oleylamine were used as ligands. The trimethylbromosilane precursor was rapidly injected into the solution of cesium acetate and manganese acetate precursor at 170 °C. After reaction for 20 s, an ice−water bath was used to

Received: June 15, 2022
Accepted: July 29, 2022
Published: August 10, 2022

put out the reaction. $CsMnBr_3$ NCs were then obtained by a centrifugation method.

Characterization. The crystal structure of the $CsMnBr_3$ SC was determined by using X-ray diffraction (XRD, Escalab 250Xi), while the morphology of NCs was analyzed by using transmission electron microscopy (TEM, JEM-2100F). Excitation and PL spectra and lifetimes were recorded by an Edinburgh FS5 spectrometer. PLQYs were obtained using an FS5 fluorescence spectrometer with an integrating sphere. The temperature-dependent PL spectra were collected from 10 to 300 K, which was excited by an He−Cd laser at 442 nm.

NLO Measurements. Our home-built microregion NLO system was used to investigate the NLO properties of $CsMnBr_3$ SC. The fs pulses at 600 and 800 nm output from TOPAS (Spectra-Physics, 1000 Hz, 100 fs) were used as resonant and nonresonant excitation sources, respectively. The PL spectra under 800 nm excitation were collected by a 20× objective lens (NA = 0.45) and then detected by the charged coupling device (SpectraPro HRS-300). The TPA coefficient of $CsMnBr_3$ SC was determined using the nonlinear transmittance method.[16]

RESULTS AND DISCUSSION

The XRD pattern of $CsMnBr_3$ SC is depicted in Figure 1a, which reveals its hexagonal crystal structure.[17] The TEM image

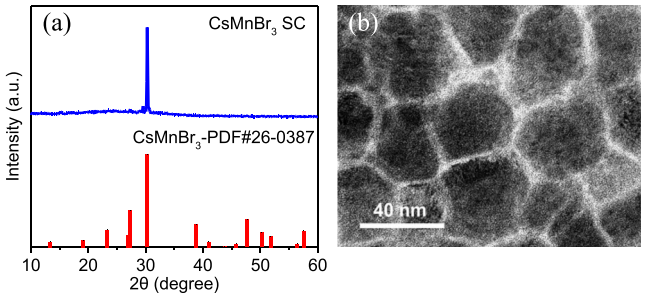

Figure 1. (a) XRD pattern of $CsMnBr_3$ SC. (b) TEM image of $CsMnBr_3$ NCs.

of $CsMnBr_3$ NCs confirms their hexagonal morphology (Figure 1b). Under the excitation of 278 nm, both $CsMnBr_3$ SC and NCs exhibit red emission, with their PL spectra peaking at ~621 and ~653 nm, respectively (Figure 2a,b). The PLQYs of $CsMnBr_3$ SC and NCs were determined as 26 and 53%, respectively. Although both the samples possess multiple peaks in the PL excitation spectra, only a single PL peak was observed. In addition, we measured excitation-wavelength-dependent PL spectra of the SC and NCs (Figure S1). It was found that the PL peaks of the two samples did not change at different excitation wavelengths, indicating that the same emissive states were involved for both of them. The PL emission for both the $CsMnBr_3$ SC and NCs was ascribed to the transition from $^4T_1$ to the ground state $^6A_1$.[7] It was found that the $CsMnBr_3$ SC still exhibited bright red emission even when it was kept at about 35% humidity for over 6 months. The time-resolved PL decay curves of $CsMnBr_3$ SC and NCs were measured at 300 K under the excitation of 422 nm (Figure 2c,d), determining their lifetimes as ~68.64 and ~240.70 μs through the monoexponential fitting. Because more defects were formed in the SC and the surface defects on the $CsMnBr_3$ NCs can be effectively passivated by the ligands, the PL lifetime of the former is much shorter than that of the

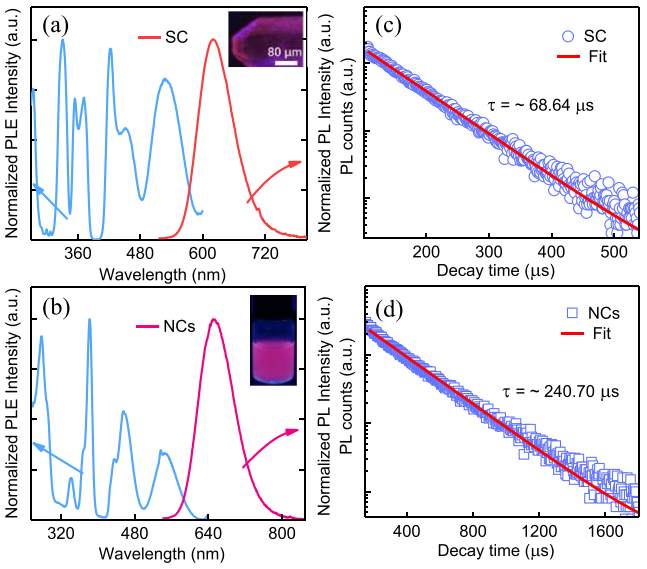

Figure 2. (a,b) Excitation and emission spectra of $CsMnBr_3$ SC and NCs. Insets: their photographs under UV light irradiation. (c,d) Time-resolved PL decay curves of $CsMnBr_3$ SC and NCs.

latter. It should be noted that the PL lifetime in our $CsMnBr_3$ NCs was much different from those in previous literature, which should be caused by the different local structures around Mn ions.[7,8]

To analyze the low-temperature optical properties of $CsMnBr_3$ SC, its PL spectra were measured as a function of temperature ranging from 10 to 300 K by using a 442 nm He−Cd laser as the excitation source (Figure 3a,b). As depicted in Figure 3c, as the temperature increases from 10 to 100 K, the PL peak of $CsMnBr_3$ SC exhibits a bathochromic shift. However, a blue shift of the PL peak was observed from 100 to 300 K. The sudden change of the PL peak energy at approximately 100 K should be associated with the occurrence of phase transition. Although the phase transition was reported in other relatively soft materials, such as the $MAPbI_3$ bulk film,[18] this is the first time that the phase transition was observed in the $CsMnBr_3$ SC. More experimental investigation was needed to further confirm the mechanism for the occurrence of phase transition in the SC.

In contrast, the PL peak of $CsMnBr_3$ NCs exhibited a monotonous blue shift with increasing temperature (Figure 3d), indicating the absence of phase transition. Actually, previous literature implied that colloidal NCs generally exhibit better thermodynamic phase stability than bulk materials, which was caused by the reduced crystal-field strength and smaller splitting energy of the excited state during thermal expansion.[8,19] Compared with the SC, the better phase stability of $CsMnBr_3$ NCs should be caused by the ligand-induced change in surface energy. Actually, such kind of stabilization phenomenon was also reported in $CH_3NH_3PbBr_3$ and $FAPbI_3$ that were modified by appropriate ligands.[20,21] Therefore, the phase transition observed in the $CsMnBr_3$ SC may be ascribed to the absence of the ligand-induced phase stabilization effect.

The change of full width at half-maximum (fwhm) of the PL spectrum is correlated with electron-phonon coupling.[22] Such an effect has been widely investigated through the measurement of temperature-dependent PL fwhm in Mn-doped perovskite NCs,[23] but it has never been reported for the $CsMnBr_3$ SC. Therefore, the PL fwhm of the $CsMnBr_3$ SC and

https://doi.org/10.1021/acsomega.2c03661
ACS Omega 2022, 7, 29415−29419

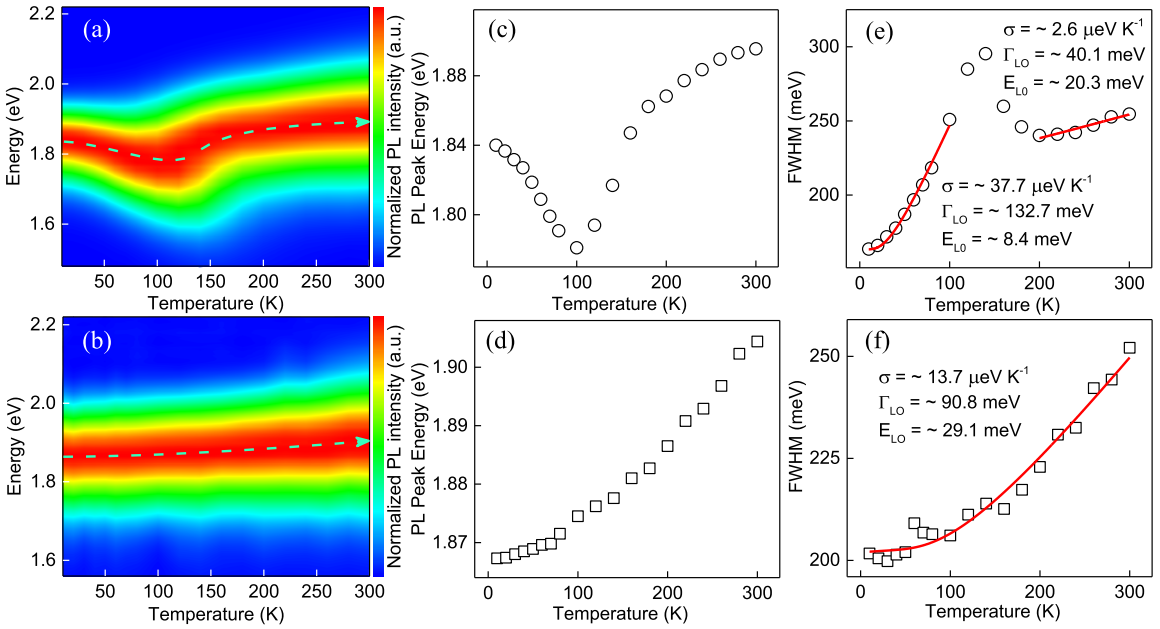

Figure 3. Pseudo-color maps of the temperature-dependent PL spectra of (a) $CsMnBr_3$ SC and (b) $CsMnBr_3$ NCs. PL peak energy and fwhm as a function of temperature for (c,e) $CsMnBr_3$ SC and (d,f) $CsMnBr_3$ NCs.

NCs at different temperatures was analyzed. As shown in Figure 3e, the PL fwhm of the $CsMnBr_3$ SC broadens at temperatures ranging from 10 to 140 and 200 to 300 K. In contrast, the PL fwhm decreases between 140 and 200 K, probably caused by the occurrence of phase transition. As expected, the PL fwhm of $CsMnBr_3$ NCs broadens monotonously as the temperature increases from 10 to 300 K (Figure 3f), which is similar to those of $CsPbX_3$ (X = Cl, Br, and I) NCs.[24] The PL fwhm as a function of temperature can be expressed as[25,26]

$$\Gamma(T) = \Gamma_{inh} + \sigma T + \Gamma_{LO}/[\exp(E_{LO}/k_B T) - 1] \quad (1)$$

where Γ_{inh} is the inhomogeneous broadening term, σ is the coupling coefficient of electron and acoustic phonon, Γ_{LO} is the coupling strength between the electron and longitudinal optical (LO) phonon, and E_{LO} is the LO phonon energy. Through theoretical fitting, for the SC at 10−100 K, σ is ∼37.7 μeV K^{-1}, while Γ_{LO} and E_{LO} are ∼132.7 and ∼8.4 meV, respectively. At 200−300 K, σ is ∼2.6 μeV K^{-1}, while Γ_{LO} and E_{LO} are ∼40.1 and ∼20.3 meV, respectively. For the $CsMnBr_3$ NCs, during the whole measured temperature range, σ is ∼13.7 μeV K^{-1}, and Γ_{LO} and E_{LO} are ∼90.8 and ∼29.1 meV, respectively. Compared with $CsMnBr_3$ NCs, the SC has stronger electron and LO phonon coupling strength at low temperatures but weaker coupling strength at high temperatures.

Next, the NLO properties of the $CsMnBr_3$ SC and NCs were comparatively investigated under resonant and nonresonant excitation (600 and 800 nm). However, no obvious NLO signals were detected in the NCs under the excitation of above two wavelengths, probably caused by the low concentration of $CsMnBr_3$ NCs (1×10^{-5} M). Considering that the SC has more advantages in the practical application of optoelectronic devices, only the NLO properties of $CsMnBr_3$ SC were studied in the following discussions. Under the resonant excitation at 600 nm, it was found that the transmittance of the $CsMnBr_3$ SC increased with increasing excitation intensity (Figure 4), confirming the occurrence of

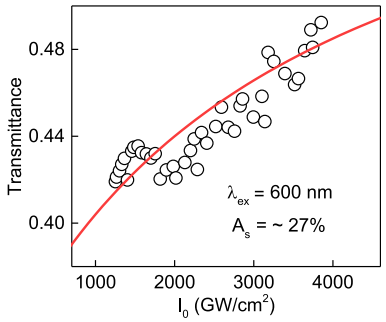

Figure 4. Excitation intensity-dependent transmittance of the $CsMnBr_3$ SC and the corresponding theoretical fitted curve under the excitation at 600 nm (100 fs, 1000 Hz).

saturable absorption. The excitation intensity-dependent transmittance of the sample can be fitted using the following formula[27]

$$T = 1 - A_s/(1 + I_0/I_{sat}) - n_s \quad (2)$$

where A_s is the modulation depth, I_0 is the incident intensity, I_{sat} is the saturable optical intensity that is required in a steady state to reduce the absorption to half of its unbleached value, and n_s is the non-saturable loss. Through the theoretical fitting using eq 2, the A_s value of the SC is determined as ∼27%, which is comparable to that of MoS_2 dispersion (∼34%, 800 nm),[28] but much larger compared with the $CsPbBr_3$ NC film (13.1%, 1060 nm).[29] Notably, the $CsMnBr_3$ SC exhibits a high damage threshold (>4000 GW cm^{-2}), implying that it is an excellent saturable absorber that may be used for Q-switching and mode-locking techniques.

Subsequently, the NLO behavior of the $CsMnBr_3$ SC under the non-resonant excitation was investigated. Bright PL emission peaking at ∼621 nm was easily observed under 800 nm excitation (Figure 5a). In addition, it was found that the PL intensity was proportional to the square of excitation power (inset of Figure 5a), confirming the TPA mechanism at 800 nm.[30] The TPA coefficient of the SC was then measured using

https://doi.org/10.1021/acsomega.2c03661
ACS Omega 2022, 7, 29415−29419

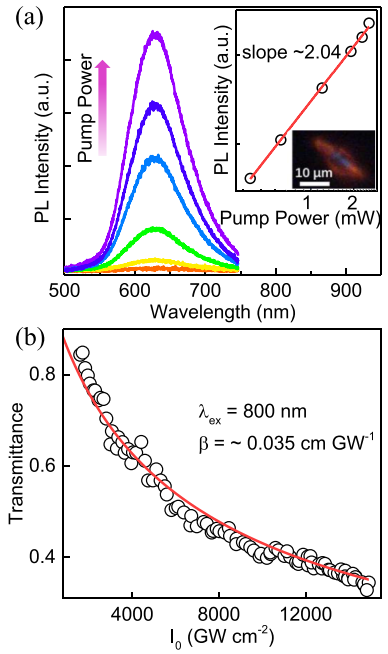

Figure 5. (a) PL spectra of the $CsMnBr_3$ SC under different excitation intensities at 800 nm (100 fs, 1000 Hz). Insets: The relationship between the PL intensity vs excitation power and the microscopic image under 800 nm excitation. (b) Transmittance under different excitation intensities and the relevant theoretical fitting curve.

the nonlinear transmittance method.[16] The corresponding experimental data are shown in Figure 5b, which can be fitted using the following equation

$$T(I_0) = [\ln(1 + I_0 L\beta)]/I_0 L\beta \quad (3)$$

where L is the thickness of the sample and β is the TPA coefficient.[16] Through the theoretical fitting, the β value of the $CsMnBr_3$ SC was determined as ~0.035 cm GW^{-1}, which is 1 order of magnitude larger than that of $Cs_3Cu_2I_5$ SC (5.1×10^{-3} cm GW^{-1}, 600 nm),[31] possibly due to the larger density of states in the former. Moreover, under the excitation intensity of 1.5×10^4 GW cm^{-2}, the transmittance can decrease to 34% and no obvious saturation effect was observed. It indicates that the $CsMnBr_3$ SC can be used as an excellent optical limiter, with a limiting threshold of ~0.9×10^4 GW cm^{-2}. It will be interesting to determine the wavelength-dependent 2PA coefficients of the $CsMnBr_3$ SC. However, we cannot obtain the 2PA coefficients at other wavelengths. Even so, the 2PA coefficient of this material was determined at the most common wavelength, that is, 800 nm, which can provide important information for the potential application in NLO devices.

CONCLUSIONS

In conclusion, we investigated the low-temperature PL spectra and NLO properties of the $CsMnBr_3$ SC. Unlike the colloidal NC counterpart, the SC underwent a phase transition at approximately 100 K, probably due to the absence of the ligand-induced phase stabilization effect. At low temperatures, the SC exhibited stronger electron and LO phonon coupling strength than that of the NCs. Notably, the $CsMnBr_3$ SC possesses excellent saturable absorption and TPA properties, indicating that it is promising for the application in Q-switching and mode-locking techniques and as an optical limiter.

ASSOCIATED CONTENT

Supporting Information

The Supporting Information is available free of charge at https://pubs.acs.org/doi/10.1021/acsomega.2c03661.

Excitation wavelength-dependent PL spectra of the $CsMnBr_3$ SC and NCs (PDF)

AUTHOR INFORMATION

Corresponding Author

Yang Gao − *Key Laboratory of Optoelectronic Devices and Systems of Ministry of Education and Guangdong Province, College of Physics and Optoelectronic Engineering, Shenzhen University, Shenzhen 518060, China;* orcid.org/0000-0003-0680-4950; Email: ygao@szu.edu.cn

Authors

Yingzhuang Xu − *Key Laboratory of Optoelectronic Devices and Systems of Ministry of Education and Guangdong Province, College of Physics and Optoelectronic Engineering, Shenzhen University, Shenzhen 518060, China*

Junzi Li − *Key Laboratory of Optoelectronic Devices and Systems of Ministry of Education and Guangdong Province, College of Physics and Optoelectronic Engineering, Shenzhen University, Shenzhen 518060, China*

Fuli Zhao − *Department of Electrical and Electronic Engineering, Southern University of Science and Technology, Shenzhen 518055, P. R. China*

Rui Chen − *Department of Electrical and Electronic Engineering, Southern University of Science and Technology, Shenzhen 518055, P. R. China;* orcid.org/0000-0002-0445-7847

Tingchao He − *Key Laboratory of Optoelectronic Devices and Systems of Ministry of Education and Guangdong Province, College of Physics and Optoelectronic Engineering, Shenzhen University, Shenzhen 518060, China;* orcid.org/0000-0003-1040-0596

Complete contact information is available at: https://pubs.acs.org/10.1021/acsomega.2c03661

Notes

The authors declare no competing financial interest.

ACKNOWLEDGMENTS

We acknowledge the financial support by the Guangdong Basic and Applied Basic Research Foundation (2019A1515012094), the Project of Department of Education of Guangdong Province (2018KTSCX198), and the Science and Technology Planning Project of Shenzhen Municipality (20200812170648001, JCYJ20190808121211510, and JCYJ 20200826143347001).

REFERENCES

(1) Zhang, Q.; Yin, Y. All-Inorganic Metal Halide Perovskite Nanocrystals: Opportunities and Challenges. *ACS Cent. Sci.* **2018**, *4*, 668−679.

(2) Guo, Z.; Li, J.; Pan, R.; Cheng, J.; Chen, R.; He, T. All-inorganic Copper(I)-Based Ternary Metal Halides: Promising Materials Toward Optoelectronics. *Nanoscale* **2020**, *12*, 15560−15576.

(3) Tan, Z.; Li, J.; Zhang, C.; Li, Z.; Hu, Q.; Xiao, Z.; Kamiya, T.; Hosono, H.; Niu, G.; Lifshitz, E.; et al. Highly Efficient Blue-Emitting

Bi-Doped Cs_2SnCl_6 Perovskite Variant: Photoluminescence Induced by Impurity Doping. *Adv. Funct. Mater.* **2018**, *28*, 1801131.
(4) Zhang, Y.; Yin, J.; Parida, M.; Ahmed, G.; Pan, J.; Bakr, O.; Bredas, J.; Mohammed, O. Direct-Indirect Nature of the Bandgap in Lead-Free Perovskite Nanocrystals. *J. Phys. Chem. Lett.* **2017**, *8*, 3173−3177.
(5) Jia, W.; Wei, Q.; Ge, S.; Peng, C.; Huang, T.; Yao, S.; Tian, Y.; Chang, T.; Zeng, R.; Zou, B. Polaronic Magnetic Excitons and Photoluminescence in Mn^{2+}-Doped $CsCdBr_3$ Metal Halides. *J. Phys. Chem. C* **2021**, *125*, 18031−18039.
(6) Peng, H.; Huang, T.; Zou, B.; Tian, Y.; Wang, X.; Guo, Y.; Dong, T.; Yu, Z.; Ding, C.; Yang, F.; et al. Organic-inorganic Hybrid Manganese Bromine Single Crystal with Dual-band Photoluminescence from Polaronic and Bipolaronic Excitons. *Nano Energy* **2021**, *87*, 106166.
(7) Almutlaq, J.; Mir, W.; Gutiérrez-Arzaluz, L.; Yin, J.; Vasylevskyi, S.; Maity, P.; Liu, J.; Naphade, R.; Mohammed, O.; Bakr, O. $CsMnBr_3$: Lead-Free Nanocrystals with High Photoluminescence Quantum Yield and Picosecond Radiative Lifetime. *ACS Mater. Lett.* **2021**, *3*, 290−297.
(8) Kong, Q.; Yang, B.; Chen, J.; Zhang, R.; Liu, S.; Zheng, D.; Zhang, H.; Liu, Q.; Wang, Y.; Han, K. Phase Engineering of Cesium Manganese Bromides Nanocrystals with Color-Tunable Emission. *Angew. Chem., Int. Ed.* **2021**, *60*, 19653−19659.
(9) Murali, B.; Kolli, H.; Yin, J.; Ketavath, R.; Bakr, O.; Mohammed, O. Single Crystals: The Next Big Wave of Perovskite Optoelectronics. *ACS Mater. Lett.* **2019**, *2*, 184−214.
(10) Wright, A.; Verdi, C.; Milot, R.; Eperon, G.; Pérez-Osorio, M.; Snaith, H.; Giustino, F.; Johnston, M.; Herz, L. Electron-Phonon Coupling in Hybrid Lead Halide Perovskites. *Nat. Commun.* **2016**, *7*, 11755.
(11) Nie, Z.; Gao, X.; Ren, Y.; Xia, S.; Wang, Y.; Shi, Y.; Zhao, J.; Wang, Y. Harnessing Hot Phonon Bottleneck in Metal Halide Perovskite Nanocrystals via Interfacial Electron−Phonon Coupling. *Nano Lett.* **2020**, *20*, 4610−4617.
(12) Li, J.; Dong, H.; Xu, B.; Zhang, S.; Cai, Z.; Wang, J.; Zhang, L. $CsPbBr_3$ Perovskite Quantum Dots: Saturable Absorption Properties and Passively Q-switched Visible Lasers. *Photonics Res.* **2017**, *5*, 457−460.
(13) Li, P.; Chen, Y.; Yang, T.; Wang, Z.; Lin, H.; Xu, Y.; Li, L.; Mu, H.; Shivananju, B.; Zhang, Y.; et al. Two-Dimensional $CH_3NH_3PbI_3$ Perovskite Nanosheets for Ultrafast Pulsed Fiber Lasers. *ACS Appl. Mater. Interfaces* **2017**, *9*, 12759−12765.
(14) Li, J.; Jing, Q.; Xiao, S.; Gao, Y.; Wang, Y.; Zhang, W.; Sun, X.; Wang, K.; He, T. Spectral Dynamics and Multiphoton Absorption Properties of All-Inorganic Perovskite Nanorods. *J. Phys. Chem. Lett.* **2020**, *11*, 4817−4825.
(15) Wang, Y.; Li, X.; Zhao, X.; Xiao, L.; Zeng, H.; Sun, H. Nonlinear Absorption and Low-Threshold Multiphoton Pumped Stimulated Emission from All-Inorganic Perovskite Nanocrystals. *Nano Lett.* **2016**, *16*, 448−453.
(16) He, G.; Reinhardt, G.; Bhatt, P.; Dillard, B.; Xu, J.; Prasad, A. Two-Photon Absorption and Optical-Limiting Properties of Novel Organic Compounds. *Opt. Lett.* **1995**, *20*, 435−437.
(17) Goodyear, J.; Kennedy, D. The Crystal Structure of $CsMnBr_3$. *Acta Crystallogr., Sect. B: Struct. Crystallogr. Cryst. Chem.* **1972**, *28*, 1640−1641.
(18) Diroll, B.; Guo, P.; Schaller, R. Unique Optical Properties of Methylammonium Lead Iodide Nanocrystals Below the Bulk Tetragonal-Orthorhombic Phase Transition. *Nano Lett.* **2018**, *18*, 846−852.
(19) Yuan, X.; Ji, S.; De Siena, M. C.; Fei, L.; Zhao, Z.; Wang, Y.; Li, H.; Zhao, J.; Gamelin, D. R. Photoluminescence Temperature Dependence, Dynamics, and Quantum Efficiencies in Mn^{2+}-Doped $CsPbCl_3$ Perovskite Nanocrystals with Varied Dopant Concentration. *Chem. Mater.* **2017**, *29*, 8003−8011.
(20) Sarang, S.; Bonabi Naghadeh, S. B.; Luo, B.; Kumar, P.; Betady, E.; Tung, V.; Scheibner, M.; Zhang, J.; Ghosh, S. Stabilization of the Cubic Crystalline Phase in Organometal Halide Perovskite Quantum Dots via Surface Energy Manipulation. *J. Phys. Chem. Lett.* **2017**, *8*, 5378−5384.
(21) Fu, Y.; Wu, T.; Wang, J.; Zhai, J.; Shearer, M. J.; Zhao, Y.; Hamers, R.; Kan, E.; Deng, K.; Zhu, X.; et al. Stabilization of the Metastable Lead Iodide Perovskite Phase via Surface Functionalization. *Nano Lett.* **2017**, *17*, 4405−4414.
(22) Gong, X.; Voznyy, O.; Jain, A.; Liu, W.; Sabatini, R.; Piontkowski, Z.; Walters, G.; Bappi, G.; Nokhrin, S.; Bushuyev, O.; et al. Electron-Phonon Interaction in Efficient Perovskite Blue Emitters. *Nat. Mater.* **2018**, *17*, 550−556.
(23) Zhang, W.; Wei, J.; Gong, Z.; Huang, P.; Xu, J.; Li, R.; Yu, S.; Cheng, X.; Zheng, W.; Chen, X. Unveiling the Excited-State Dynamics of Mn^{2+} in 0D Cs_4PbCl_6 Perovskite Nanocrystals. *Adv. Sci.* **2020**, *7*, 2002210.
(24) Zhao, F.; Li, J.; Gao, X.; Qiu, X.; Lin, X.; He, T.; Chen, R. Comparison Studies of the Linear and Nonlinear Optical Properties of $CsPbBr_xI_{3-x}$ Nanocrystals: The Influence of Dimensionality and Composition. *J. Phys. Chem. C* **2019**, *123*, 9538−9543.
(25) Lee, J.; Koteles, E.; Vassell, M. Luminescence Linewidths of Excitons in GaAs Quantum Wells Below 150 K. *Phys. Rev. B: Condens. Matter Mater. Phys.* **1986**, *33*, 5512−5516.
(26) Rudin, S.; Reinecke, T.; Segall, B. Temperature-Dependent Exciton Linewidths in Semiconductors. *Phys. Rev. B: Condens. Matter Mater. Phys.* **1990**, *42*, 11218−11231.
(27) Zheng, Z.; Zhao, C.; Lu, S.; Chen, Y.; Li, Y.; Zhang, H.; Wen, S. Microwave and Optical Saturable Absorption in Graphene. *Opt. Express* **2012**, *20*, 23201−23214.
(28) Zhang, H.; Lu, S.; Zheng, J.; Du, J.; Wen, S.; Tang, D.; Loh, K. Molybdenum Disulfide (MoS_2) as a Broadband Saturable Absorber for Ultra-fast Photonics. *Opt. Express* **2014**, *22*, 7249−7260.
(29) Zhou, Y.; Hu, Z.; Li, Y.; Xu, J.; Tang, X.; Tang, Y. $CsPbBr_3$ Nanocrystal Saturable Absorber for Mode-Locking Ytterbium Fiber Laser. *Appl. Phys. Lett.* **2016**, *108*, 261108.
(30) He, G.; Tan, L.-S.; Zheng, Q.; Prasad, P. N. Multiphoton Absorbing Materials: Molecular Designs, Characterizations and Applications. *Chem. Rev.* **2008**, *108*, 1245−1330.
(31) Guo, Z.; Li, J.; Gao, Y.; Cheng, J.; Zhang, W.; Pan, R.; Chen, R.; He, T. Multiphoton Absorption in Low-Dimensional Cesium Copper Iodide Single Crystals. *J. Mater. Chem. C* **2020**, *8*, 16923−16929.

https://doi.org/10.1021/acsomega.2c03661
ACS Omega 2022, 7, 29415−29419